Thermal behaviour of ytterbium-doped fluorite crystals under high power pumping

Justine Boudeile, Julien Didierjean, Patrice Camy, Jean-Louis Doualan, Abdel Abdel.Benayad@ensicaen.Fr Benayad, Vivien Ménard, Richard Moncorgé, Frédéric Druon, François Balembois, Patrick Georges

Thermal behaviour of ytterbium-doped fluorite crystals under high power pumping

J. Boudeile,[1*] J. Didierjean,[1] P. Camy,[2] J. L. Doualan,[2] A. Benayad,[2] V. Ménard,[2] R. Moncorgé,[2] F. Druon,[1] F. Balembois[1] and P. Georges[1]

[1]*Laboratoire Charles Fabry de l'Institut d'Optique, CNRS, Univ. Paris-Sud,Campus Polytechnique, RD 128, 91127 Palaiseau Cedex*

[2]*Centre de recherche sur les Ions, les Matériaux et la Photonique (CIMAP), CNRS 6252 CEA-CNRS-ENSI Caen, Université de Caen, 6 Boulevard Maréchal Juin, 14050 Caen Cedex*

**Corresponding author: justine.boudeile@institutoptique.fr*

Abstract: We report an *in situ* thermal study of Yb-doped fluorite crystals Yb:CaF_2 and Yb:SrF_2 under high power pumping, with or without laser operation. The experiment combines simultaneously thermography and measurement of the thermal aberrations. This setup allows us to measure temperature gradients, thermal lens, and absorption coefficients. From these measurements, we evaluate the thermal conductivity, fractional thermal load, and thermo-optic coefficient. Great differences are observed between the lasing and non lasing regimes. Our measured thermal lenses are greater than what are expected from the thermo-optic parameters found in previous work. Based on this thermal study, we design a laser cavity operating with large output power and TEM_{00}, leading to better performances for Yb:CaF_2 than Yb:SrF_2.

OCIS codes: (120.6810) Thermal effects; (140.3480) Lasers, diode-pumped; (140.3615) Lasers, ytterbium.

References and links

1. P. Camy, J. L. Doualan, A. Benayad, M. von Edlinger, V. Ménard, and R. Moncorgé, "Comparative spectroscopic and laser properties of Yb^{3+}-doped CaF_2, SrF_2 and BaF_2 single crystals," Appl. Phys. B **89,** 539-542 (2007).
2. A. Lucca, G. Debourg, M. Jacquemet, F. Druon, F. Balembois, P. Georges, P. Camy, J. L. Doualan, and R. Moncorgé, "High-power diode-pumped Yb^{3+}:CaF_2 femtosecond laser," Opt. Lett. **29**, 2767-2769 (2004), http://www.opticsinfobase.org/abstract.cfm?URI=ol-29-23-2767
3. A. Lucca, M. Jacquemet, F. Druon, F. Balembois, P. Georges, P. Camy, J. L. Doualan, and R. Moncorgé, "High-power tunable diode-pumped Yb^{3+}:CaF_2 laser," Opt. Lett. **29**, 1879-1881 (2004), http://www.opticsinfobase.org/abstract.cfm?URI=ol-29-16-1879.
4. V. Petit, J. L. Doualan, P. Camy, V. Ménard, and R. Moncorgé, "CW and tunable laser operation of Yb^{3+} doped CaF_2," Appl. Phys. B **78**, 681-684 (2004).
5. M. Siebold, J. Hein, M. C. Kaluza, and R. Uecker, "High-peak-power tunable laser operation of Yb:SrF_2," Opt. Lett. **32**, 1818-1820 (2007), http://www.opticsinfobase.org/abstract.cfm?URI=ol-32-13-1818
6. M. Siebold, M. Hornung, S. Bock, J. Hein, M.C. Kaluza, J. Wemans and R. Uecker, "Broad-band regenerative laser amplification in ytterbium-doped calcium fluoride (Yb:CaF_2)," Appl. Phys. B **89,** 543-547 (2007).
7. M. Weber, *Handbook of Optical Materials*, (CRC Press LLC, 2003).
8. R. Gaumé, B. Viana, D. Vivien, J. P. Roger, and D. Fournier, "A simple model for the prediction of thermal conductivity in pure and doped insaluting crystals," Appl. Phys. Lett. **83,** 1355-1357 (2003).
9. B. M. Mogilevskii, V. F. Tumnuroma, A. F. Chudnovskii, E. D. Kaplan, L. M. Puchkina and V. M. Reiterov, "Thermal conductivity of fluorides of alkali earth metals," J. Eng. Phys. and Thermo. **30,** 210-214 (1976).
10. S. Chénais, F. Balembois, F. Druon, G. Lucas-Leclin, and P. Georges, "Thermal lensing in Diode-pumped Ytterbium Lasers - Part I: Theoretical Analysis and Wavefront Measurements," IEEE J. Quantum Electron. **40,** 1217-1234 (2004).
11. T. M. Jeong, D. -K. Ko, and J. Lee, "Method of reconstructing wavefront aberrations by use of Zernike polynomials in radial shearing interferometers," Opt. Lett. **32**, 232-234 (2007), http://www.opticsinfobase.org/abstract.cfm?URI=ol-32-3-232
12. J. Didierjean, E. Herault, F. Balembois, P. Georges "Thermal conductivity measurements of laser crystals by infrared thermography. Application to Nd:doped crystals," accepted for publication in Optics Express

#94782 - $15.00 USD Received 7 Apr 2008; revised 21 May 2008; accepted 22 May 2008; published 23 Jun 2008

13. S. Chénais, S. Forget, F. Druon, F. Balembois and P. Georges, "Direct and absolute temperature mapping in diode-end pumped Yb:YAG," Appl. Phys. B **79,** 221-224 (2004).
14. T. Y. Fan, "Heat generation in Nd:YAG and Yb:YAG", IEEE J. Quantum Electron. **29**, 1457-1459 (1993).
15. F. Augé, F. Druon, F. Balembois, P. Georges, A. Brun, F. Mougel, G. Aka, and D. Vivien, "Theroretical and Experimental Investigations of a Diode-Pumped Quasi-Three-Level Laser: The Yb^{3+}-doped $Ca_4GdO(BO_3)_3$ (Yb:GdCOB) Laser," IEEE J. Quantum Electron. **36**, 598-606 (2000).

1. Introduction

More and more industrial applications require efficient, reliable and compact laser configurations. Diode-pumped systems are very promising in this respect. Since the emergence of very high-power laser diodes emitting around 980 nm, most investigations are focused on diode-pumped Yb^{3+}-doped materials. Because of their simple electronic energy-level scheme, no undesired effects like up-conversion, concentration quenching, cross-relaxation and excited-state absorption are expected, thus reducing the thermal load. Moreover, the quantum defect is generally 10 % for ytterbium ions, compared to 25 % for neodymium ions. Despite these advantages, an excellent thermal conductivity of the Yb^{3+}-hosts is preferable for high average power scaling. This is one of the reasons why fluorite crystals are very promising, with thermal conductivity values equal to 9.7, 8.9 $W.m^{-1}.K^{-1}$ for CaF_2 and SrF_2 respectively [1]. These values are comparable to the 11 $W.m^{-1}.K^{-1}$ value for a YAG crystal.

Yb^{3+}-doped fluorite crystals mix the advantages of crystals and glasses since they combine an excellent thermal conductivity and a broad emission spectrum At high dopant concentrations, the substitution of Ca^{2+}or Sr^{2+} ions by Yb^{3+} ions produces clusters inside the matrix, thereby broadening the emission spectrum. This allowed the demonstration of femtosecond oscillators [2], CW-tunable lasers or quasi-CW-tunable lasers [3-5] and regenerative amplifiers [6]. Finally, these crystals are easily grown in large size by Bridgman, Czochralski or temperature-gradient methods, yielding good optical quality material.

Although undoped fluorite properties are fairly well-known, Yb-doped compounds are not fully characterised, and their thermal behaviour in laser configuration have never been studied to our knowledge. This point is however very important for laser development. In particular, the design of high power laser cavities with good beam quality requires the knowledge of the induced thermal lens.

In this letter, we present a complete thermal study of Yb^{3+}:MeF_2 (where Me = Ca and Sr) under high power pumping, in the presence or absence of laser effect. The experimental characterization setup combines simultaneously thermal mapping and wavefront measurement. These measurements allow us to evaluate the fractional thermal load, the radiative quantum efficiency, the laser extraction efficiency, and the thermo-optic coefficient, for the first time to our knowledge for Yb-doped fluorites. These measured values of the thermo-optic coefficient are compared to values calculated for the undoped crystals thanks to the available spectroscopic parameters in the literature. Finally, the measured thermal lenses were used to optimize a high-power laser cavity for both Yb^{3+}-doped CaF_2 and SrF_2 crystals.

2. Spectroscopic parameters and crystallographic data for fluorite crystals

The spectroscopic parameters and crystallographic data of Yb^{3+}:MeF_2 (where Me = Ca and Sr) are summarized in table 1, and the emission and absorption spectra of each fluorite crystal are plotted on Fig. 1 [1, 7]. We notice a better calculated value of the thermal conductivity for the Yb^{3+}:CaF_2 compared to the value for Yb^{3+}:SrF_2.

#94782 - $15.00 USD Received 7 Apr 2008; revised 21 May 2008; accepted 22 May 2008; published 23 Jun 2008

Table 1: Spectroscopic parameters and crystallographic data for the fluoride crystals

	Yb:CaF_2	**Yb:SrF_2**
doping concentration	2.6 %	2.9 %
absorption peak (nm)	979.8	976.5
absorption cross-section σ_{abs} (10^{-21} cm^2)	5.4	9.1
lifetime τ (ms)	2.4	2.9
thermal conductivity κ_c ($W.m^{-1}.K^{-1}$) (doped crystals)	**6.06* (Yb:2.6%)**	**3.43*(Yb:2.9%)**
	CaF_2	**SrF_2**
refractive index n	1.43	1.438
density d ($g.cm^3$)	3.181	4.276
molecular mass ($g.mol^{-1}$)	78.08	125.62
cell volume (10^{-30} m^3)	163.04	195.11
undoped thermal conductivity ($W.m^{-1}.K^{-1}$)	9.7	8.3
dn/dT (10^{-6} K^{-1})	-10.6	-12.0
thermal expansion α_T (10^{-6} K^{-1})	18.9	18.4
Poisson's ratio ν	0.28	0.25
C_r	-0.098	-0.125
C_θ	-0.1025	-0.131
χ (dn/dT)	-10.6 10^{-6} K^{-1}	-12.0 10^{-6} K^{-1}
χ (stress) = $2.n^3.\ \alpha_T.\ C_{r,\theta}$	-11.1 10^{-6} K^{-1}	-14 10^{-6} K^{-1}
χ (dilatation) = $(n-1)(1+\nu)\ \alpha_T$	10.4 10^{-6} K^{-1}	10.1 10^{-6} K^{-1}
$\chi = \chi$ (dn/dT)+ χ (stress)+ χ (dilatation)	**-11.3 10^{-6} K^{-1}***	**-15.9 10^{-6} K^{-1}***

*calculated from [8,9,10]

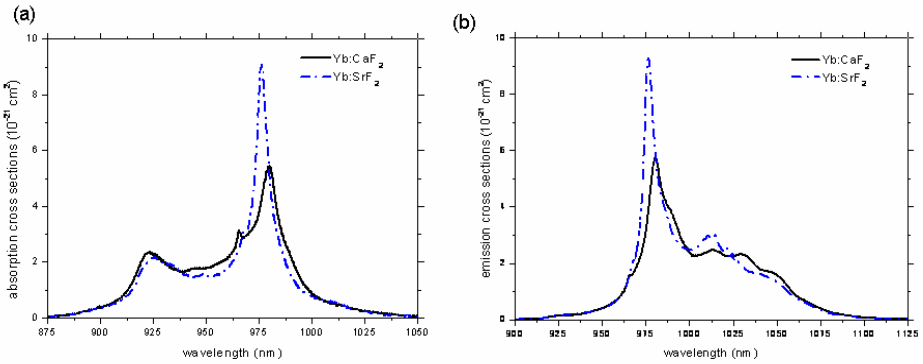

Fig. 1. Absorption (a) and emission (b) spectra of the Yb^{3+}:MeF_2 (where Me=Ca and Sr)

3. Experimental setup for the thermal characterization

The experimental setup is shown in Fig. 2. The crystals are directly pumped with a 120 W 400-µm core fiber-coupled laser diode (LIMO) emitting at 980 nm with an N.A. of 0.22. The pump beam is collimated and focused into the gain medium using 60 mm focal-lengths doublets. The crystal is placed on a water-cooled copper mount with a contact for cooling on three sides. The laser cavity is a Rmax-plano (M_1) – Rmax-concave (M_3, RoC = 200 mm) resonator. The back mirror (M_1) is a dichroïc mirror allowing to longitudinally pumping the crystal. This cavity is folded twice to allow simultaneous analysis of the crystal temperature map and thermal aberrations.

#94782 - $15.00 USD Received 7 Apr 2008; revised 21 May 2008; accepted 22 May 2008; published 23 Jun 2008

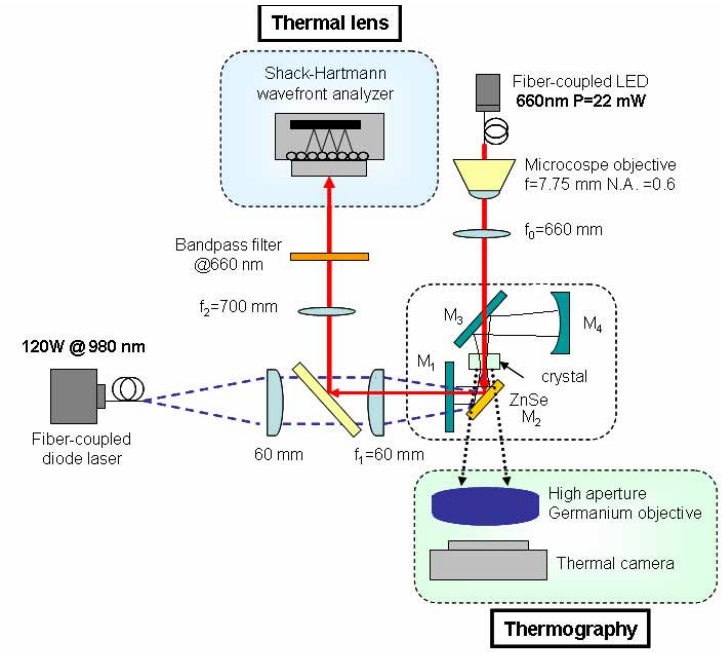

Fig. 2. Experimental setup for thermal characterizations.

The flat folded plan mirror (M_3) is inserted inside the laser cavity to avoid defocusing of the wavefront probe beam (red beam in Fig. 2). The probe beam, generated by a fiber-coupled LED emitting at 660 nm, is collimated and superposed with the pump and laser beams. The wavelength is chosen at 660 nm, outside any absorption or emission bands of the laser crystals. The probe is also chosen because of its high spatial coherence (to correctly define the reference wavefront) and its low temporal coherence (to avoid coherent cross talk, which corresponds to the interference between two neighbouring microlens diffraction patterns in the Shack-Hartmann wavefront analyzer). An uncoated glass plate is inserted in the pump beam path to reflect part of the probe to the detector. The facet of the crystal is imaged through a magnifying system composed of two lenses (f_1=60mm and f_2=700 mm) to a Shack-Hartmann wavefront sensor (HASO 64®, Imagine Optics) [10]. A bandpass filter at 660 nm is placed in front of the analyzer to remove any parasitic IR beams. A reference wavefront is recorded with the pump off to cancel all the static aberrations from the optical elements and the unheated crystal, allowing the precise measurement of thermally induced wavefront deformations. The spatial phase is reconstructed by projection on the set of the orthogonal Zernike circle polynomials [11]

The second folded mirror in the laser cavity (M_2) is a plate of Zinc Selenium (ZnSe). This plate is coated to reflect the pump and laser wavelengths and to transmit in the far IR wavelength region and introduces the mean losses in the laser cavity [12]. An 8 µm-12 µm sensitive high resolution (60 µm) thermal camera with a high aperture (N.A. = 0.7) germanium objective is used to measure the temperature map of the pumped facet of the crystal [13].

Although fluorite crystals are well-known to be transparent in a large wavelength domain (from far IR to VUV), the high Yb doping concentration induces absorption in the wavelength range of the thermal camera (8-12 µm). The residual transmission in this IR band is measured to be 5 % for a 200°C source behind the 0.5-mm Yb(2.9%):CaF_2. The absorption coefficient at these wavelengths is found equal to α_p=60 cm^{-1}. The thermal radiation measured by the IR

#94782 - $15.00 USD Received 7 Apr 2008; revised 21 May 2008; accepted 22 May 2008; published 23 Jun 2008

camera is therefore emitted from the first 150 µm which can be considered as the pumped input facet.

An important advantage of this experimental setup resides in the possibility of performing a thermal study in laser operating conditions or not. For highly pumped Yb-doped crystals, the pump absorption saturation induces very different behaviour in the presence or absence of laser effect.

4-Results of the thermal experiment

4.1- Temperature elevation

The thermography images at maximum pump powers are shown in Fig. 3. The temperature images clearly indicate a good cooling efficiency since no important hot spot is observed. The measurements are summarized in Table 2. To avoid crystal fracture of SrF_2, the incident pump power is limited to 47 W under laser operation.

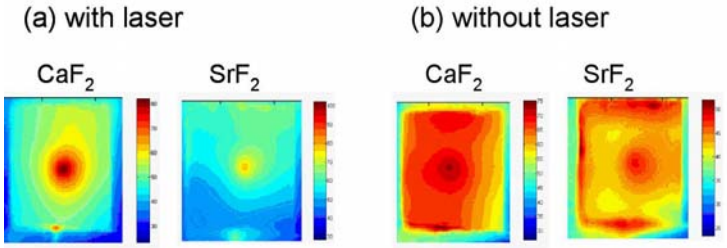

Fig. 3. Thermography of Yb^{3+}:$CaF_2$and Yb^{3+}:SrF_2 (a) with laser operation and (b) without laser operation at maximum pump power. The cooled sides are right left and bottom.

Table 2: Temperature gradient and global temperature elevation for Yb^{3+}:CaF_2 and Yb^{3+}:SrF_2

	with laser operation		Without laser operation	
Crystals	**Yb:CaF_2**	**Yb:SrF_2**	**Yb:CaF_2**	**Yb:SrF_2**
Incident power	83 W	47 W	83 W	47 W
Absorbed power	40 W	18 W	32 W	10 W
w_p^2	220 µm	220 µm	220 µm	220 µm
temperature gradient (ΔT)	**34°C**	**26°C**	**13°C**	**6°C**
T_{max}	**82°C**	**79°C**	**67°C**	**48°C**

We note large pump absorption variation in the presence or absence of laser effect: 9.6% for Yb:CaF_2 and 17% for Yb:SrF_2. This explains the different measured values of temperature gradients: a higher absorbed power induces a higher temperature gradient.

The temperature gradients without laser effect are low, so that reduced thermal lensing effects are expected. In contrast, under laser operation, temperature gradients increase (more than 25 °C) and strong thermal lensing effects probably occur. These strong variations between the two regimes need to be taken into account during the laser alignment process. They even lead to thermal shock-induced crystal fracture if no special care is taken.

4.2 Wavefront distortion

The thermal dioptric power of the pumped crystal versus absorbed pump power is plotted in Fig. 4 for CaF_2 and SrF_2 crystals with or without laser operation. We notice that all thermal dioptric powers (D_{th}) are negative leading to thermal divergent lenses (f_{th}) for both crystals. This result can be understood as follows. The thermal dioptric power can be expressed as [10]:

#94782 - $15.00 USD Received 7 Apr 2008; revised 21 May 2008; accepted 22 May 2008; published 23 Jun 2008

$$D_{th} = \frac{1}{f_{th}} = \frac{\eta_h P_{abs}}{2\pi w_p^2 \kappa_c}\left[\left(\frac{dn}{dT}\right) + (n-1)(1+\nu)\alpha_T + 2n^3\alpha_T C_r\right] = \frac{\eta_h P_{abs}\chi}{2\pi w_p^2 \kappa_c} \quad (1)$$

where η_h is the fractional thermal load, P_{abs} the absorbed pump power, w_p the pump beam waist radius, κ_c the thermal conductivity, n the refractive index, ν the Poisson's ratio, α_T the coefficient of thermal expansion, C_r the photo-elastic constant, χ the thermo-optic coefficient and T the temperature. The absolute values of the $(n\text{-}1)(1+\nu)\alpha_T$ and $2n^3\alpha_T C_r$ terms are similar and compensate each other (Table 1). The sign of D_{th} is therefore almost determined by the term (dn/dT). Since the values of (dn/dT) for the CaF_2 and SrF_2 are equal to -10.6 10^{-6} $K^{-1}$and -12 10^{-6} K^{-1} respectively, divergent thermal lenses are expected.

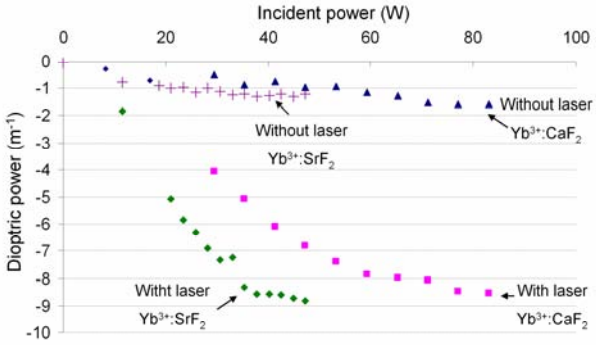

Fig. 4. Dioptric power versus incident power for CaF_2:Yb^{3+} and SrF_2:Yb^{3+}

The thermal focal lengths for Yb^{3+}:CaF_2 and Yb^{3+}:SrF_2 are equal to -119 mm and -113 mm for absorbed powers of 40 W and 18 W respectively. We observed a crystal fracture limit power around 90 W for Yb:CaF_2. Since both fluorite crystals have similar values of thermal expansions α_T but SrF_2 has a lower thermal conductivity than CaF_2 (Table 1), we restricted the pump power on the Yb:SrF_2 in order to avoid fracture with this crystal. The pump power was adjusted to have the same range of thermal focal lengths in both crystals.

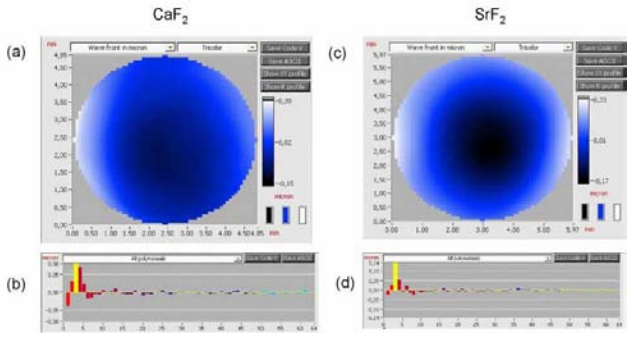

Fig. 5. Amplitude of wavefront distortion (a) and (c) and corresponding Zernike polynomial decomposition (b) and (d) for Yb^{3+}:CaF_2 and Yb^{3+}:SrF_2 at maximal incident pump power, respectively; in the polynomial decomposition the yellow bar represents the focus.

#94782 - $15.00 USD Received 7 Apr 2008; revised 21 May 2008; accepted 22 May 2008; published 23 Jun 2008

The wavefront distortion for each fluorite crystal is shown in Figs. 5(a) and 5(c) under laser conditions. The peak to valley distance is equal to 0.289 µm and 0.370 µm for $CaF_2:Yb^{3+}$ and $SrF_2:Yb^{3+}$ respectively.

5. Determination of the intrinsic parameters of Yb-doped fluorite crystals

The evaluation of intrinsic parameters is carried out in the following manner. First, the thermal conductivity is evaluated from the thermal maps under laser operation. Then, we study the heat sources in these crystals [14]. To this end, we introduce the fractional thermal load $\eta_{h(with\ laser)}$, which corresponds to the fraction of the pump power converted in heat by the following expression:

$$\eta_{h(\ with\ \ laser\ )} = 1 - \eta_p \left[(1-\eta_l)\eta_r \frac{\lambda_p}{\lambda_f} + \eta_l \frac{\lambda_p}{\lambda_l} \right] \tag{2}$$

where λ_p is the pump wavelength, λ_l the laser wavelength, λ_f the average fluorescence wavelength. The excitation pump efficiency η_p is the number of excited ions in their emitting state per absorbed pump photon. The laser extraction efficiency η_l stands for the fraction of excited ions giving rise to laser emission. The radiative quantum efficiency η_r represents the number of spontaneously emitted photons per excited ion. From the determination of heat sources in the crystal, we are able to calculate the value of the thermo-optic coefficient.

5.1 Thermal conductivity κ_c for Yb-doped fluorite crystals

Following the method described in [12], the thermal conductivities of fluorite crystals are evaluated to be 5.4 ± 1 $W.m^{-1}.K^{-1}$ and 3.1 ± 0.4 $W.m^{-1}.K^{-1}$ for CaF_2:Yb(2.6%) and SrF_2:Yb(2.9%) respectively. Theses values are close to the calculated values of thermal conductivity in table 1 and comfort us about the values used in simulation as we can observe on Fig. 6.

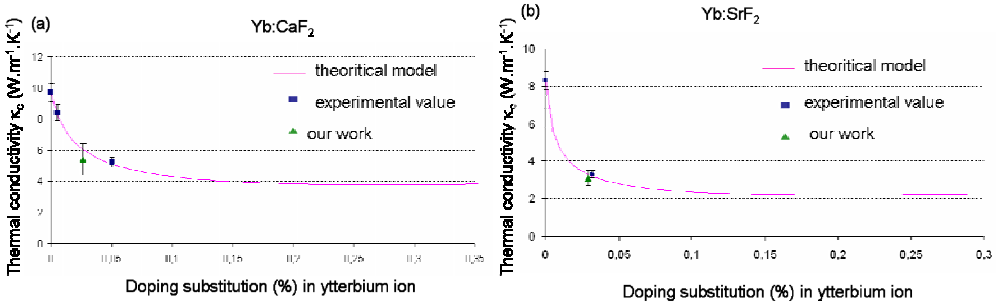

Fig. 6. Thermal conductivity for (a) $Yb:CaF_2$ and (b) $Yb:SrF_2$

5.2 Determination of heat sources in Yb-doped fluorite crystals

The unsaturated absorption coefficients α_{NS} are key parameters in the following, and were measured to be 340 and 420 m^{-1} for $Yb:CaF_2$ and $Yb:SrF_2$ respectively by strongly attenuating the pump beam. We start by determining the fractional thermal load $\eta_{h(without\ laser)}$. Since the pumping volume is cylindrical and the crystal size is large compared to the pumping beam, the crystal can be accurately considered as a cylinder for the theoretical model. We note *r* the radial coordinate. The radius of the crystal is $r_0=2mm$. The fractional thermal load $\eta_{h\ (without\ laser)}$ is obtained from the temperature map without laser action through the following equations involving the temperature gradient ΔT [11]:

#94782 - $15.00 USD Received 7 Apr 2008; revised 21 May 2008; accepted 22 May 2008; published 23 Jun 2008

$$\Delta T = T(r,z) - T(r_0,z) = -\frac{\eta_{h(\text{without laser})}}{4\pi\kappa_c}\frac{dP(z)}{dz} f(r,z)$$

$$f(r,z) = \begin{cases} \ln\left(\frac{r_0^2}{w_p^2(z)}\right) + 1 - \frac{r^2}{w_p^2(z)} & x \le w_p(z) \\ \ln\left(\frac{r_0^2}{r^2(z)}\right) & r > w_p(z) \end{cases} \quad (3)$$

where $dP(z)/dz$ is the evolution of the pump power inside the crystal. Absorption saturation is taken into account, under non-lasing operation, by the following equation for $I_p(z)$ which is the pump power divided by the spot area:

$$\frac{dI_p(z)}{dz} = \frac{-\alpha_{NS} I_p(z)}{1 + I_p(z)/I_{psat}} = \frac{-\alpha_{NS} I_p(z)}{1 + \left[(\sigma_{abs}(\lambda_p) + \sigma_{em}(\lambda_p))\tau\right]} \quad (4)$$

where I_{psat} is the pump saturation irradiance, α_{NS} the unsaturated absorption coefficient, $\sigma_{abs}(\lambda_p)$ the absorption cross-section at the pump wavelength, $\sigma_{em}(\lambda_p)$ the emission cross-section at pump wavelength and τ the emission lifetime. The measured absorbed pump power and unsaturated absorption coefficient allow us to evaluate $dP(z)/dz$ through Eq. (4). The experimental (blue points) and theoretical (red line) temperature maps without laser operation are plotted in Fig. 7. The only parameter used to adjust both curves is the fractional thermal load $\eta_{h\ (without\ laser)}$ which are 0.033 and 0.013 for CaF_2 and SrF_2 respectively. This difference between both crystals can be explained by the fact that, in the absence of laser operation, the heat is mainly due to the quantum defect between the pump and fluorescence wavelengths. Since the value of the average fluorescence wavelength λ_f is lower in SrF_2 than in CaF_2 (table 3), it is expected to find a smaller value for $\eta_{h\ (without\ laser)}$ in the case of SrF_2.

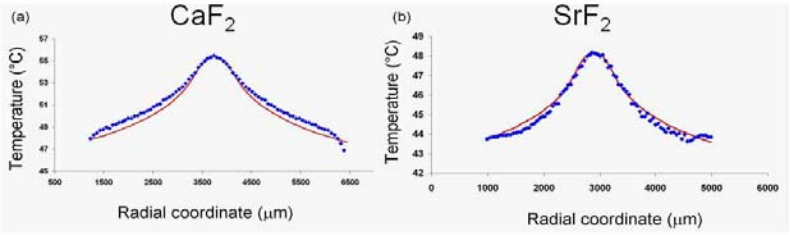

Fig. 7. Experimental (bleu points) and the corresponding theoretical (red line) temperature profiles at z=0 for (a) Yb^{3+}:CaF_2 and for (b) $Yb^{3+}SrF_2$

From the fractional thermal load $\eta_{h\ (without\ laser)}$, we deduce the radiative quantum efficiency η_r:

$$\eta_{h(\text{without laser})} = 1 - \eta_p \eta_r \frac{\lambda_p}{\lambda_f} \quad (5)$$

#94782 - $15.00 USD Received 7 Apr 2008; revised 21 May 2008; accepted 22 May 2008; published 23 Jun 2008

A non-unity pump quantum efficiency η_p may be related to the excitation of non-luminescent (dead) or non-radiative sites. In the case of our high quality Yb-doped fluorite crystals impurities and defect centers are very much reduced, and η_p is considered equal to unity.
The parameters and results obtained are summarized in Table 3:

Table 3. Table of parameters and results obtained.

Crystals	$Yb^{3+}:CaF_2$	$Yb^{3+}:SrF_2$
$\sigma_{abs}(\lambda_p)$	5.4 10^{-21} cm²	7.1 10^{-21} cm²
$\sigma_{em}(\lambda_p)$	5.0 10^{-21} cm²	5.0 10^{-21} cm²
$dP(z)/dz$	3669	3110
$\eta_{h\ (without\ laser)}$	**0.035**	**0.014**
λ_f	1008 nm	989 nm
η_r	**0.993**	**0.995**
λ_l	1053 nm	1051 nm
$\eta_{h(with\ laser)}$	**0.050**	**0.039**

We note the η_r values are close to unity. This means that the excited ions which do not participate to laser emission will mainly contribute to spontaneous emission, and that in the absence of laser operation, the heat source is due to the quantum defect between the pump and fluorescence wavelengths. This heat source is close to the minimal value for a crystal. This is corroborated by the low measured temperature gradients and dioptric power when the laser is not operating.

Knowing η_r we are able now to determine the value of the laser extraction efficiency η_l [10]:

$$\eta_l(r) \approx \frac{\sigma_{em}(\lambda_l) I(r)}{\sigma_{em}(\lambda_l) I(r) + (1/\eta_r \tau)} \tag{6}$$

where $\sigma_{em}(\lambda_l)$ is the emission cross-section at the laser wavelength λ_l and $I(r)$ the intracavity laser intensity. $I(r)$ is expressed in unit of photons.s^{-1}.cm^{-2} by [15]:

$$I(r) = \frac{2.\lambda_l.P_{int}}{hc\pi.w_c^2} exp\left\{-2r^2/w_c^2\right\} \tag{7}$$

where h is the Planck constant, c the speed of light in vacuum, w_c the laser beam waist, P_{int} the intracavity laser power and r the radial position in the crystal. The approximated Eq. (6) is valid in our case since reabsorption at the laser wavelength is negligible [10]. The laser extraction efficiency η_l is plotted versus the radial coordinate for both crystals in Fig. 8.

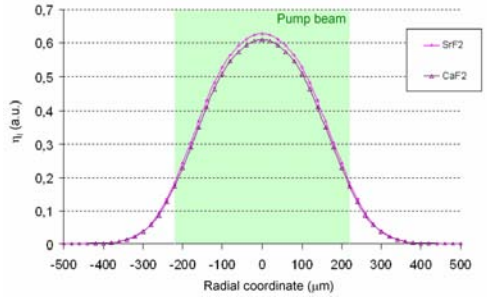

Fig. 8. Laser extraction efficiency for $Yb^{3+}:CaF_2$ (triangles) and $Yb^{3+}:SrF_2$ (circles).

#94782 - $15.00 USD Received 7 Apr 2008; revised 21 May 2008; accepted 22 May 2008; published 23 Jun 2008

The spatially averaged values for η_l are 0.45 and 0.46 for Yb^{3+}:CaF_2 and Yb^{3+}:SrF_2 respectively. These are obtained by performing an average weighted by the pump intensity profile (which is top-hat in our case due to the multimode fiber coupled pump diode). Weak intracavity powers explain non-unity values for the laser extraction efficiencies. The intracavity losses are mainly due to the presence of the ZnSe plate in the laser cavity and the absence of antireflection coating on the crystals [14].

We can now easily determine the fractional thermal coefficient with laser operation using Eq. (2). The fractional thermal loads are summarized in Table 3.

It is also possible to calculate η_h with laser directly thanks to the thermal profiles obtained under laser operation. By fitting these curves, we have obtained the values summarized in Table 4. The two methods to obtain $\eta_{h(with\ laser)}$ (calculated from η_h without laser or directly fitting the thermal profile with laser operation) give very similar results and corroborate each other (Table 3- Table 4).

Table 4. Table of parameters and results obtained with thermographies under laser operation.

Crystals	Yb^{3+}:CaF_2	Yb^{3+}:SrF_2
dP(z)/dz with laser	8131	4996
$\eta_{h(with\ laser)\ thermography}$	**0.055**	**0.042**

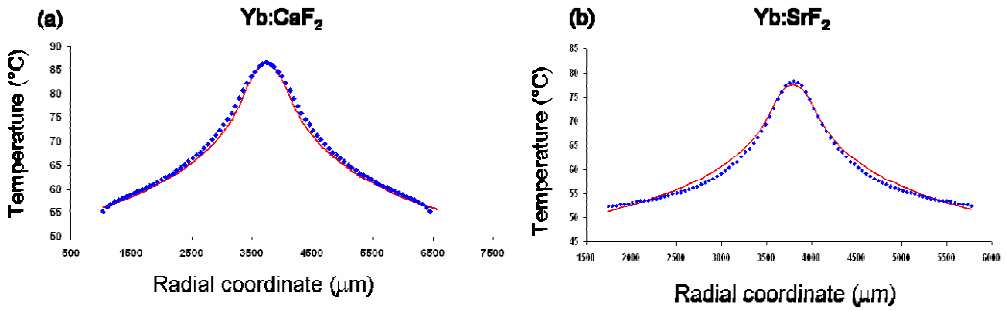

Fig. 9. Experimental (bleu points) and the corresponding theoretical (red line) temperature profiles at z=0 for (a) Yb^{3+}:CaF_2 and for (b) $Yb^{3+}SrF_2$ under laser operation.

In conclusion, in the absence of laser operation, the amount of heat in the crystal is very low because it is almost only due to the quantum defect between the pump and fluorescence wavelengths. In case of laser operation, the heat is created by the quantum defect: approximately half from the fluorescence and half from the laser photons. In this case the laser emission generates more heat than the fluorescence emission (table 3). These reasons, added to strong absorption saturation of the pump, explain important differences of heating occurring with and without laser operation.

5.3 Determination of the thermo-optic coefficient χ

Using the Eq. (1), the only parameter we can adjust to fit the measured dioptric power is the thermo-optic coefficient. In these conditions, χ is measured to be $-17.8\ 10^{-6} \pm 1.5\ 10^{-6}\ K^{-1}$ and $-20.5\ 10^{-6} \pm 1.8\ 10^{-6}\ K^{-1}$ for Yb^{3+}:CaF_2 and Yb^{3+}:SrF_2 respectively.

#94782 - $15.00 USD Received 7 Apr 2008; revised 21 May 2008; accepted 22 May 2008; published 23 Jun 2008

Table 5. Comparison between the experimental and theoretical results

Crystals	$Yb^{3+}:CaF_2$	$Yb^{3+}:SrF_2$
χ *theoretical* K^{-1} *(undoped crystal)*	$-17.8 \pm 1.5\ 10^{-6}$	$-20.5 \pm 1.8\ 10^{-6}$
χ *experimental* K^{-1} *(doped crystals)*	$-11.3\ 10^{-6}$	$-15.9\ 10^{-6}$
f_{th} *theoretical mm (undoped thermal conductivity)*	-302*	-364**
f_{th} *theoretical mm (doped thermal conductivity)*	-188*	-158**
f_{th} *experimental mm (doped thermal conductivity)*	-119	-113

*$\eta_p=\eta_r=1$; $\eta_h= 0.045$; $\eta_l= 0.45$; $\chi= -11.3\ 10^{-6}\ K^{-1}$

**$\eta_p=\eta_r=1$; $\eta_h= 0.037$; $\eta_l= 0.46$; $\chi= -15.9\ 10^{-6}\ K^{-1}$

One can notice that there is an important difference between our evaluation of the thermo-optic coefficient and the theoretical one found in the literature for undoped fluorite crystals (Table 5). Two mechanisms can explain this difference: 1) the variations of the thermo-optic parameters with the doping concentration, 2) the thermo-optic coefficient given in the literature is calculated when the crystal is at thermodynamical equilibrium and at constant strain. However in our experiments, the thermo-optic coefficients are measured when the crystal is pumped, thus far from the thermodynamical equilibrium.

To conclude, in the context of Yb-doped crystal laser media, the use of published values of the thermo-optic coefficients for undoped crystals leads to an underestimation of thermal lensing effect. In our case, the difference is 37 % for $Yb^{3+}:CaF_2$ and of 38 % for $Yb^{3+}:SrF_2$. The measured values obtained in this work therefore allow proper optimization of high-power laser cavities based on fluorite crystals, as shown in next section.

6. High average power laser cavities

The laser cavity is a simple V-shaped resonator [Fig. 10(a)]. The oscillator is composed of a planar dichroïc mirror (M_a), a concave mirror with a radius of curvature of 200 mm (M_b) and a planar output coupler of 10 % for $Yb^{3+}:SrF_2$ and 15 % for $Yb^{3+}:CaF_2$ (M_c). The crystal is considered like a divergent lens with a thermal focus length of -113 mm for $Yb^{3+}:SrF_2$ and -119 mm for $Yb^{3+}:CaF_2$. The optimal distances between the different optical elements are estimated using an ABCD matrix-based software. The output power is plotted versus the incident power in Fig. 10(b).

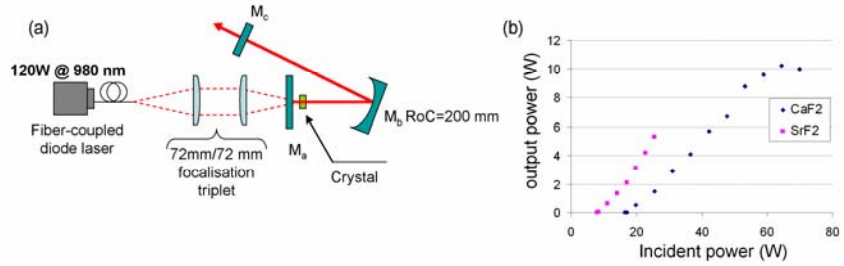

Fig. 10. (a). Laser cavity design (b) output power versus incident power.

An output average power of 5.8 W, [Fig. 8(b)] is obtained for 26 W of incident pump power (absorbed power of 20 W) for $Yb^{3+}:SrF_2$. The slope efficiency (output power versus diode pump power) is 22.7 % and the optical-optical efficiency is 21.1 %. The incident pump power is limited to 26 W to avoid crystal fractures.

#94782 - $15.00 USD Received 7 Apr 2008; revised 21 May 2008; accepted 22 May 2008; published 23 Jun 2008

With the Yb^{3+}:CaF_2 crystal, an average output power of 10.2 W [Fig. 10(b)] is obtained for 64 W of incident pump power, corresponding to an absorbed power of 39 W and an intracavity power of about 68 W. The slope efficiency is 21.6 % and the optical-optical efficiency is 16 %. A roll-off in average output power [Fig. 10(b)] is observed when approaching crystal fracture. The laser beam is almost diffraction-limited at 64 W of incident pump power, with M^2 factors equal to 1.16 and 1.20 along the x and y directions respectively (Fig. 11). To our knowledge this is the highest average output power ever obtained for a diode-pumped Yb-doped CaF_2 laser in CW regime.

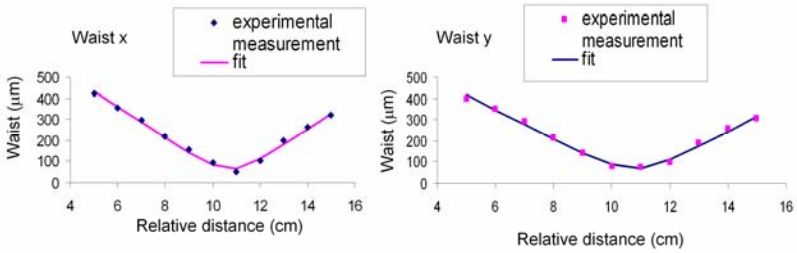

Fig. 11. M^2 factors along the x and y directions for Yb:CaF_2

7. Conclusion

In conclusion, we report a complete thermal study of Yb-doped fluorite crystals Yb^{3+}(2.6%):CaF_2 and Yb^{3+}(2.9%):SrF_2 in the context of high-power pumped laser. This is carried out using an experimental setup which combines simultaneously temperature mapping and thermal lens measurements, both in the presence and absence of laser effect. These measurements allowed us to retrieve intrinsic parameters of the doped crystals, leading to values different from previously published values for undoped crystals. Based on this study, we designed high power single-transverse-mode laser cavities, and obtained the highest reported output power in CW for such lasers. Due to a higher thermal conductivity and lower thermo-optic response, Yb^{3+}:CaF_2 exhibits better performances than Yb^{3+}:SrF_2 in the context of high average power CW lasers.

Acknowledgments

This work has been partially funded by the MRCT/CNRS national research network CMDO+ (http://cmdo.cnrs.fr) and the Optics Valley network PRISM.

#94782 - $15.00 USD Received 7 Apr 2008; revised 21 May 2008; accepted 22 May 2008; published 23 Jun 2008